CRYSTAL GROWTH & DESIGN

Article

pubs.acs.org/crystal

In Situ Observation of Biotite Dissolution at pH 1 Using Advanced Optical Microscopy

Chiara Cappelli,*[,†] Alexander E. S. Van Driessche,[§] Jordi Cama,[‡] and F. Javier Huertas[†]

[†]Instituto Andaluz de Ciencias de la Tierra (IACT - CSIC-Universidad de Granada), Avda. de las Palmeras 4, 18100 Armilla, Granada, Spain

[‡]Institute of Environmental Assessment and Water Research (IDAEA), CSIC, Jordi Girona 18-26, 08034 Barcelona, Spain

[§]Laboratorio de Estudios Cristalograficos (IACT, CSIC-Universidad de Granada), Avd. de las Palmeras 4, 18100 Armilla, Granada, Spain

Web-Enhanced Feature

ABSTRACT: Laser confocal microscopy with differential interference contrast microscopy (LCM-DIM) was used to study in situ the biotite (001) basal surface dissolution performing long-term flow-through experiments at pH 1 (T = 11.5−70 °C). Time-lapse image sequences of large areas (up to 1 mm) of the evolving cleavage (001) surface showed that dissolution only occurs at surface edges. In addition, in contrast to an observed rapid dissolution at low steps (few layers), swelling and contraction of the edge layers occurred at high steps (many layers). An increase in temperature enhanced the surface edge dissolution from 7.5×10^{-4} μm s^{-1} at 11.5 °C to 6.2×10^{-2} μm s^{-1} at 70 °C. The results obtained in this work demonstrate that LCM-DIM is a powerful technique to study in situ the dissolution mechanism and kinetics of phyllosilicates.

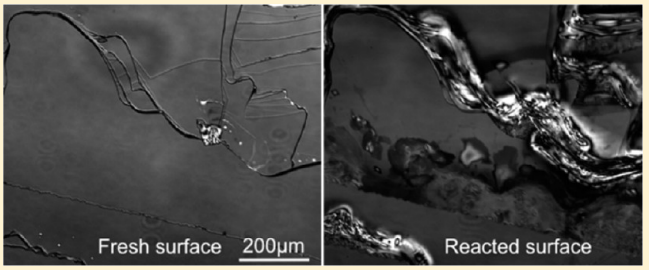

1. INTRODUCTION

Kinetics of phyllosilicate dissolution has been extensively studied over the last 20 years.[1] In particular, special attention has been paid to understand the effect that pH exerts on the dissolution mechanisms and rate. It is argued that at acidic pH clay mineral dissolution predominantly takes place at the clay mineral edge surface.[2] The interesting research on dissolution of kaolinite[3] and biotite, using powder samples[4,5] and single crystals (monolithes),[6] showed that the contribution of the edge surface area to the dissolution rate is higher than the basal surface area, suggesting that the edge sites dissolve faster than sites on the basal surface and often control the overall dissolution rate under acidic conditions. After these initial studies, atomic force microscopy (AFM) has been the most frequently used technique to investigate, at the nanoscale, the reaction mechanisms of phyllosilicates dissolution. Rufe and Hochella[7] assessed quantitatively the reactive surface area of dissolving phlogopite at acidic conditions and room temperature. Although the basal {001} surfaces showed certain reactivity, the dissolution rates normalized to the edge surface area were 2 orders of magnitude faster than rates normalized to the total surface area for this mineral. Bosbach et al.[8] and Bickmore et al.[9] showed that the basal surfaces of two smectite (hectorite and nonotronite) crystallites appeared to be unreactive during the time scale of the experiments in acid solutions. At high temperature (100−140 °C), Aldushin et al.[10] investigated the reactions of phlogopite and apophyllite with acidic solutions and observed that phlogopite dissolution occurred via nucleation of etch pits on the pristine surface, implying that the basal surface plays an important role in the dissolution processes, at least at elevated temperatures. The apophyllite basal surface underwent a swelling process forming square-shaped hillocks. McMaster et al.[11] and Haward et al.[12] suggested that etch pit nucleation at the biotite basal plane controls the biotite dissolution in the presence of oxalic acid. In the absence of oxalate, however, formation of discrete etch-pits at room temperature was not observed. Pachana et al.[13] based on SEM and AFM examinations observed stair-shaped etch pits on muscovite and biotite during hydrothermal (200 °C) alteration in acidic solutions (pH 1.1−5.7) and identified the role that nanogenic coating phases exert on the control of mineral alteration.

On the basis of these previous studies, one can assume that the likely mechanism controlling biotite dissolution at acidic pH (in the absence of oxalate) is the retreat of the sheet edge parallel to basal cleavage, resulting in an almost inert basal surface during dissolution. From the two types of biotite surface, the basal (001) and the edge (lateral) (hk0), the latter is dominantly involved. However, it appears that at high temperature the formation of etch pits contributes to the biotite dissolution at the basal surface,[13] in contrast to the absence of etch pits formation at ambient temperature (10−35 °C).[11,12]

Within this context, it still remains unclear whether the formation of etch pits at the biotite basal surface during biotite

Received: February 20, 2013
Revised: May 17, 2013

   dx.doi.org/10.1021/cg400285a | *Cryst. Growth Des.* XXXX, XXX, XXX−XXX

dissolution at acid pH could intervene in the overall reaction. As formation of etch pits at the basal surface is apparently temperature dependent, the study is conducted from 11.5 to 70 °C. In the previous studies, biotite (and other mica) dissolution at acid pH was investigated from macroscopic to nanoscopic perspectives based on the solution chemistry from flow-through cells with powder samples and AFM observations on biotite surfaces. Nonetheless, systematic, in situ, and real time exploration of broad regions of the reacting biotite (001) cleavage surface (in the order of tens of thousands square micrometers) is still lacking.

To this end, the recently developed noninvasive laser confocal microscopy with differential interference contrast microscopy (LCM-DIM) technique[14] allows in situ surface exploration with vertical nanometric accuracy at different temperatures.[15] LCM-DIM has been successfully applied to investigate in situ crystal-growth processes of gypsum crystals in a broad temperature and supersaturation range.[16] Although unambiguous quantitative information on the vertical surface topography is unavailable with LCM-DIM, horizontal quantification is possible, and measurements of step edge retreat with time can be performed. This type of observation benefits from the advantage that broad surface regions can be scanned for long time periods and allows the visualization of the mechanisms on surface areas with variable roughness and topography. A new temperature controlled flow-through cell was incorporated in the experimental microscope setup to examine the alteration of the biotite (001) cleavage surface during long-term experiments (up to 6 days) at pH 1 and temperature range from 11.5 to 70 °C.

2. MATERIALS AND METHODS

2.1. Experimental Setup. Changes on biotite (001) cleavage surface topography were monitored in situ employing LCM-DIM.[14]

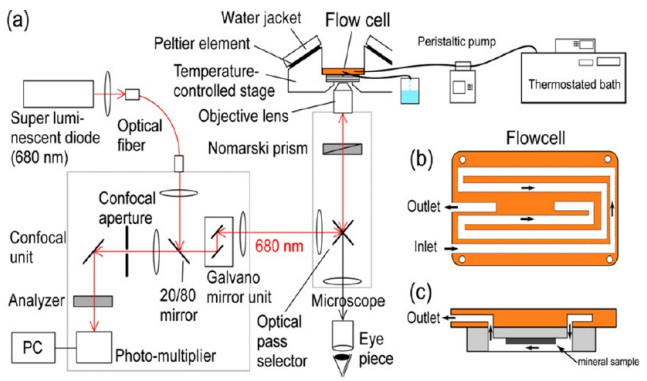

Figure 1. Schematic representation of the experimental setup: (a) the LCM-DIM equipment, (b) top view and (c) a cross-sectional view of the temperature-controlled observation flow cell.

This advanced optical system (Figure 1a) is a combination of two microscopy techniques: a confocal system (FV300, Olympus) is attached to an inverted optical microscope (IX70, Olympus), and a Nomarski prism is introduced into the optical path. A partially coherent super luminescent diode (Amonics Ltd., model ASLD68-050-B-FA: 680 nm) is used to eliminate diffraction noise. This combination provides high contrast and high resolution in the vertical plane ($z \sim 1$ nm) of the crystal surface, and the $x-y$ plane resolution is ~1380 nm for a 10× objective lens (LUCplan FLN 10×, Olympus).[15] The surface is scanned line-by-line deflecting the laser beam in the $x-y$ plane by galvanic mirrors. The light reflected at the crystal surface/solution interface is detected by a photomultiplier tube (PMT).

A custom-made Teflon flow-through cell consisted of a rectangular prism with a volume of 0.08 cm^3 and a fissure on one side. The observation cell was mounted inside a copper sample stage which completely surrounds the cell, except for the observation area (7 mm in diameter) at the bottom side (Figure 1b,c). To precisely control the temperature of the sample stage, a curve-matched thermistor and two Peltier elements were employed. Moreover a PR-59 (Supercool) temperature controller PC-interfaced through a serial connection by means of a Labview driver was used. Water jackets with circulating water were placed on top of the Peltier hot sides to increase the cooling capacity for set points below room temperature. Thermal silicon grease was employed to minimize thermal contact resistance. The precision of the temperature control is ±0.5 °C.[17]

2.2. Dissolution Experiments. The biotite used in the present study is from Bancroft (Ontario, Canada) and was purchased from Ward's Natural Science Establishment. In principle, its composition and structural formula should be similar to that reported by Turpault and Trotignon (1994)[6] who used a similar biotite sample.

In the flow-through experiments, biotite flakes with (001) cleavage surfaces of ~2 × 8 mm^2 and between 0.08 and 0.15 mm in thickness reacted with 0.1 mol L^{-1} HNO_3 (~ pH 1) and 0.01 mol L^{-1} $NaNO_3$ solutions prepared from ultrapure grade chemicals.

To observe the dissolving basal surface, the samples were fixed parallel to the (001) surface on the bottom of the fissure of the reactor cell by a silicone adhesive (Figure 1c). A small canal on each side of the cell allowed circulation of the reacting solution at a constant flow rate (0.01−0.07 mL min^{-1}), yielding a residence time from approximately 1 to 8 min. The Teflon reactor was carefully sealed with a cover glass glued with high vacuum grease (Dow Corning). The experiments were conducted at pH ~ 1 over a wide temperature range (11.5−70 °C). To increase the thermal stability in the experiments at $T \geq 40$ °C, the reacting solutions were preheated in a thermostatted bath (Figure 1a). Additionally, the input solutions were degasified with a vacuum pump for ~2 h to reduce bubble formation during the high temperature runs ($T \geq 40$ °C).

Experiments lasted from 2 h to 6 days according to the experimental conditions (i.e., the lower the temperature, the longer the experiment span due to the slower biotite dissolution kinetics). Images of the (001) cleavage surface were taken every 20 s to 15 min with a time of capture of 9.6 s. Replicas were performed for each experiment. Retreat rate (R_r) at a given location of the surface was computed from the surface horizontal retreat: $R_r = \Delta L/(t_2 - t_1)$, where ΔL is the change in the surface horizontal length as measured over the period between t_1 and t_2 at a given location.

3. RESULTS AND DISCUSSION

3.1. Biotite Dissolution Mechanism. The LCM-DIM images show that the freshly cleaved biotite (001) surface is a flat basal surface formed by terraces of variable extension and height (Figure 2a). The limit between terraces is marked by lines; high steps display darker outlines (A-A′, B−B′, C−C′, and D-D′ in Figure 2a) than lower ones (e-e′, f-f′, and g-g′ in Figure 2a). The visible limits of the (001) cleavage planes do not show preferential crystallographic directions. Surface changes are readily visible as the biotite surface interacts with the pH 1 solution. It is observed that the retreat of the higher steps occurs rather irregularly along the edge as dissolution starts. For instance, the evolution of a high step is depicted in the images of Figure 2 (experiment B50−1−2, Table 1): the terraces of the pristine surface are limited by high (AA′, BB′, CC′, and DD′) and low (ee′, ff′, and gg′) steps (Figure 2a). After 53 min at 50 °C (Figure 2b), alteration of the high steps is only visible at limited sections, resulting in a localized step alteration and stationary step position. In the altered sections, the upper layers appear "overexposed" (black arrows) due to swelling and consecutive breaking that induce the process of layer peeling. After ~6 h of reaction only the step edges AA′

dx.doi.org/10.1021/cg400285a | Cryst. Growth Des. XXXX, XXX, XXX−XXX

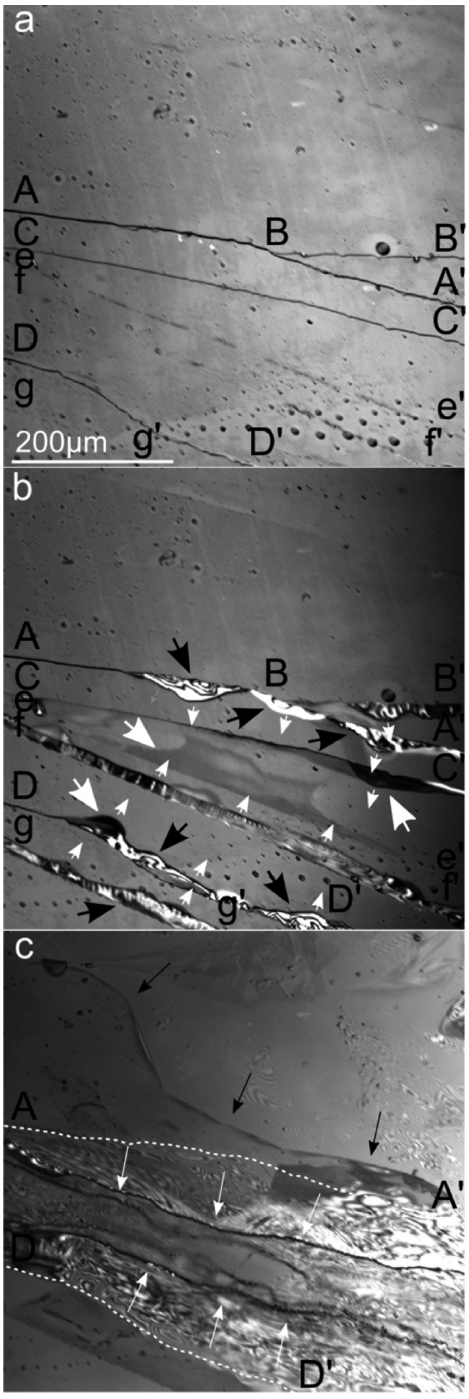

Figure 2. LCM-DIM images of biotite (001) cleavage surface: pristine surface (a), same surface reacted for 53 min (b) and ~6 h (c) at pH 1 and 50 °C. Capital letters and lower case letters indicate high and low step edges, respectively. Dissolution of higher steps at early stages of the reaction moves nonhomogeneously inward from the edges. The spherical structures in (a) are air bubbles adsorbed on the surface. Large white and black arrows in (b) indicate swelling and peeling layers, respectively, while small white arrows indicate dissolution directions. During the first hour of the reaction, the steps do not retreat, suggesting some dissolution of the upper layers. As the reaction continues, most of the steps disappear to leave altered areas. Two uniform reaction fronts remain after 6 h (AA′ and DD′ in c). Dotted lines in (c) indicate the AA′ and DD′ step positions after 53 min; white arrows show dissolution directions, and black arrows indicate dissolution of a new low step leaving fresh surface.

Table 1. Experimental Conditions

experiment	T (°C)	HNO_3 (M)	$NaNO_3$ (M)	flow rate (mL min^{-1})	duration (h)
B11.5-1-1	11.5	0.1	0.01	0.072	141.8
B11.5-1-2	11.5	0.1	0.01	0.072	89.8
B25-1-3	25	0.1	0.01	0.072	31.0
B25-1-4	25	0.1	0.01	0.072	18.3
B40-1-1	40	0.1	0.01	0.073	4.3
B40-1-1c	40	0.1	0.01	0.073	3.7
B50-1-1	50	0.1	0.01	0.01	97.6
B50-1-2	50	0.1	0.01	0.01	25.2
B70-1-3	70	0.1	0.01	0.068	4.8
B70-1-3b	70	0.1	0.01	0.068	2.1
B70-1-5b	70	0.1	0.01	0.072	2.0

and DD′ are visible, remaining stable along the main part of its length (Figure 2c). Yet, the altered areas spread following uniform reaction fronts and originated a widely degraded region. The other high and lower steps disappear either after complete dissolution of a terrace or after coalescence into the main steps.

In general, the retreat of the step edges follows an approximately normal direction to the terrace limits, irrespective of the experimental temperature (Figure 3). Figure 3a shows the altered biotite cleavage surface after 5 h of dissolution at 70 °C (experiment B70-1-1, Table 1) with the presence of several steps of relatively low height. After 30 min of reaction, the steps have retreated and left a fresh new basal biotite surface (Figure 3b). The advance of the reaction front occurs approximately normal to the edge (indicated by white arrows). Nevertheless, inspection of the position of the reaction fronts (e.g., f_1 and f_2 in Figure 3) at discrete consequent intervals shows that they move at different velocities (see the change in the f_1−f_2 distance with time), yielding a dissolution-front fluctuation likely caused by local surface defects (e.g., chemical inhomogeneities). In Figure 3 likewise, it is observed that upper layers move faster than lower ones and promote the formation of new surface edges (see black arrows in Figure 3c). This behavior mostly indicates step−step interaction.[10]

Figure 4 shows a sequence of images obtained during an experiment performed at 11.5 °C for 6 days (experiment B11.5-1-1, Table 1). After 21 h dissolution takes mainly place at discrete sections along the steps (Figure 4a,b). Swelling and peeling also occur, and the retreat of lower steps leaves altered areas (Figure 4c). Interestingly, dissolution at the basal plane is visible (Figure 4c,d). Swelling of basal surface precedes the contraction and breaking of the layers (Figure 4c). The origin of this behavior is unclear and could depend on the presence of nonvisible defects in the basal plane. Figure 5 (experiment B25-1-4, Table 1) shows that the existence of small holes (indicated by black arrow), likely caused by the previous cleaving of the basal surface, could act as surface features that significantly promote dissolution by generating fronts spreading from these structures. Therefore, although this phenomenon can contribute to the overall dissolution rate, the dissolution of basal planes starting from these preexistent defects cannot be considered as etch pits nucleation and growth. This particular mechanism may be analogous to the defect-controlled mechanism observed in chlorite by Brandt et al. (2003).[18]

Mica dissolution is thought to be dominated by an edge attack mechanism that produces selective leaching of interlayer (K^+, Na^+) and octahedral (Mg^{2+}, Fe^{2+}, Fe^{3+}, Al^{3+}) cations

dx.doi.org/10.1021/cg400285a | Cryst. Growth Des. XXXX, XXX, XXX−XXX

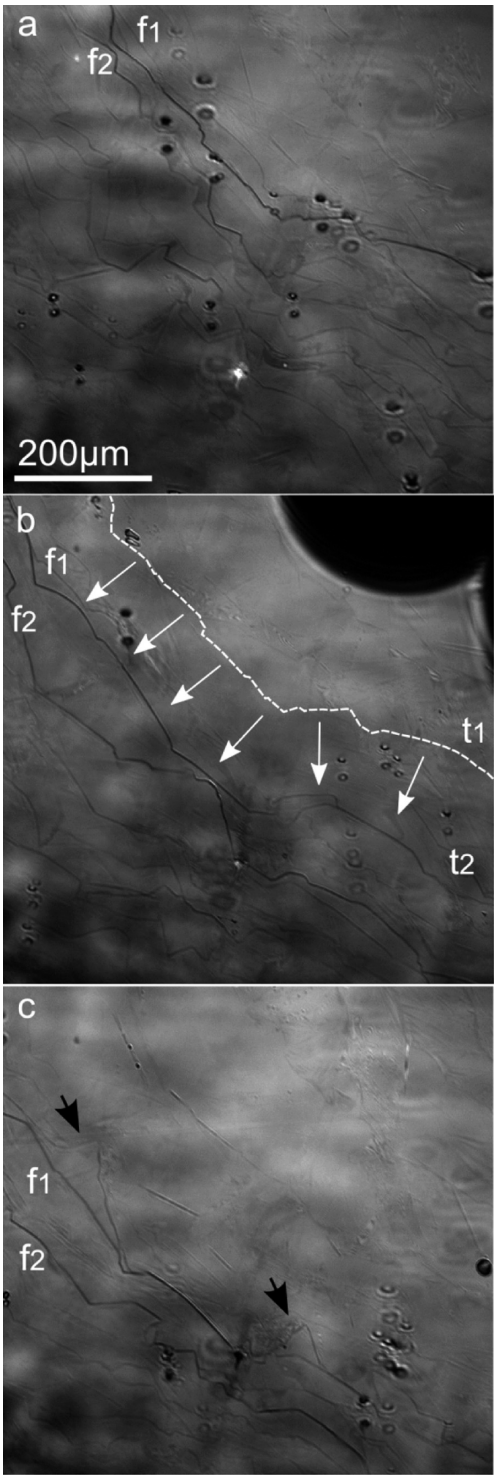

Figure 3. LCM-DIM images of reacted biotite (001) cleavage surface after ~5 h (t_1) (a), 5 h and 30 min (t_2) (b), and 5 h and 46 min (c) at pH 1 and 70 °C. In (b) the dotted line indicates the previous position of the main edge in (a). White arrows indicate retreat direction. Black arrows in (c) indicate areas where upper layers dissolved faster than the lower ones. The different distance between consecutive dissolution fronts for different time reactions (f_1 and f_2 in a, b, and c) is indicative of retreat fluctuation. The small dark spherical structures and the large dark area in the upper right corner in (b) are air bubbles; the pale elliptic structures are dust particles derived from the objective lens. A time-lapse movie of this process in AVI format is available in the HTML version.

through the {*hk*0} surfaces and forms an altered silica-enriched rim.[4,6,7,10,19] Fast exchange of interlayer potassium by protons and loss of octahedral cations lead to biotite layers curling and peeling off.[6] Atomic force microscopy (AFM) revealed a change in the phlogopite layer volume induced by alteration in HCl solutions at pH 2 that was explained by depolymerization and repolymerization reactions occurring during leaching layer formation.[7] After the initial leaching of octahedral cations, the hydrolysis of Si−O−Si and Si−O−Al in the tetrahedral sheet allows the layer to expand. The consecutive cross-linking of neighboring Si−OH groups to reform Si−O−Si (repolymerization) might cause layer contraction by the expulsion of water. Aldushin et al.[10] observed that the dissolution of phlogopite basal surface at 100−135 °C was accompanied by an alteration of the topmost layers. Initially the layer expands and then corrugates and decomposes. They interpreted the mechanism as Rufe and Hochella[7] but did not observe contraction of the depolymerized layers likely due to the higher alteration temperature.

The current observation is substantially consistent with these previous studies, and the topographical changes in biotite can be explained by initial leaching of interlayered and octahedral cations, followed by depolymerization and polymerization of tetrahedral sheet. These reaction stages lead to swelling and peeling of the uppermost layers in higher steps and formation of a degraded, low reflective surface, associated with the residual silica-rich layer and biotite incongruent dissolution. The retreat of low steps that leave a fresh basal surface can be interpreted as congruent dissolution.

The above results show that the dissolution mechanism of the biotite (001) cleavage surface is the same for the entire temperature range of this study and that formation of etch pits does not occur. This is consistent with the study by Rufe and Hochella[7] who etched the phlogopite surface with HF to produce an edge surface and did not observe the nucleation of etch pits on the {001} surfaces. On the other hand, McMaster et al.[11] show that dissolution of the biotite (001) surface in oxalic acid is dominated by the formation of etch pits, but in the absence of oxalate the formation of discrete etch pits is not observed.

3.2. Biotite Dissolution Rate. Steps of different thickness retreat at different rates. As expected, higher steps retreat more slowly than the lower ones. For example, in the experiment conducted at 50 °C and pH 1 (B50-1-2, Figure 2), the retreat rate of the higher steps (e.g., AA′ and DD′) is 5.4×10^{-3} μm s^{-1}, whereas that of the lower steps, that dissolves leaving fresh surface (see black arrows) is 2.6×10^{-2} μm s^{-1}. On the basis of the LCM-DIM measurements of the horizontal low steps retreat variation with time, dissolution rates of the biotite (*hk*0) surface were obtained at different temperatures.

In fact, the low-steps variation with time was considered to be optimal to quantify the retreat rates because they actually correspond to the dissolution of a few layers.[10] Hence, the horizontal retreat rates (R_r in μm s^{-1}) were obtained with an estimated error of 25% (standard deviation calculated from the step retreat values of replicated experiments) (Table 2). The Arrhenius plot derived from the rates with temperature yields an apparent activation energy (E_{app}) of 61.7 kJ mol^{-1} (Figure 6). This value suggests that biotite dissolution at pH 1 is surface controlled.[20]

It is not easy to compare the retreat rates obtained in this study with the rates reported in two previous studies that dealt with the dissolution of the biotite basal surface at acid pH.[12,13]

dx.doi.org/10.1021/cg400285a | *Cryst. Growth Des.* XXXX, XXX, XXX−XXX

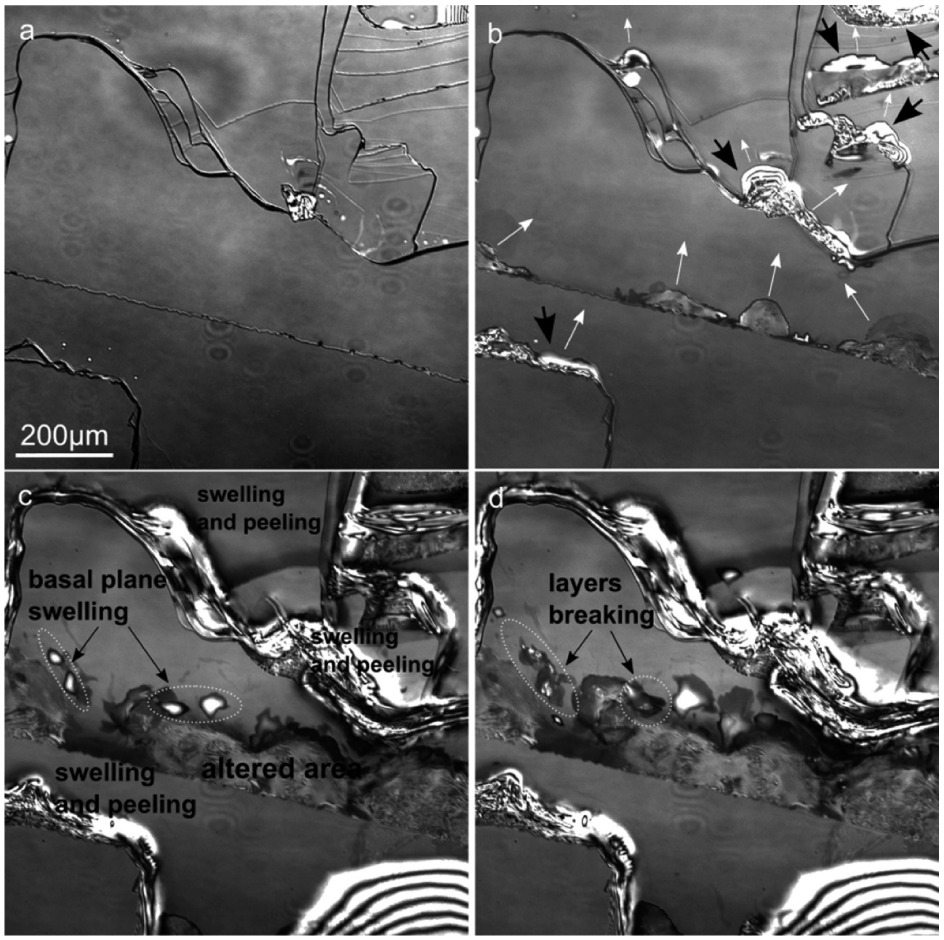

Figure 4. LCM-DIM images of biotite (001) cleavage surface: pristine surface (a) and after reaction at pH 1 and 11.5 °C for 21 h (b), ~5 days (c), and ~6 days (d). Note the presence of high step edges (dark outlines). Dissolution started irregularly along the edges (white arrows in (b) indicate dissolution direction). Large black arrows indicate overlighted areas (regions with PMT saturation) where roughening and peeling of layers occur. A time-lapse movie of the last 42 h of the experiment is available.

The main difficulty arises from the fact that the basal surface dissolution was controlled by the etch pit formation in the presence of oxalate and at high temperature (200 °C). However, the E_{app} value inferred from the step-retreat rates falls in the E_{app} range associated with etch pit growth into the {hk0} surfaces.

4. CONCLUSIONS

This study demonstrates the following:

(1) LCM-DIM is a powerful noninvasive optical technique to investigate in situ the topographic changes on dissolving mineral surface areas over a broad temperature range. Hence, this technique is useful to unravel the major dissolution mechanisms of phyllosilicates.

(2) On the basis of the time-lapse high-resolution image sequences, biotite dissolution is mainly controlled by surface-edge retreat. Dissolution from existing defects on the basal plane is not a proper biotite dissolution mechanism. Formation of basal etch pits did not occur during the reaction time of the experiments (up to 6 days) in the temperature range of this study (11.5−70 °C).

(3) The apparent activation energy value of 61.5 kJ mol^{-1} suggests that biotite dissolution at pH 1 is surface controlled.

■ ASSOCIATED CONTENT

Ⓦ Web-Enhanced Feature

Time-lapse movies of Figures 3 and 4 in AVI format.

■ AUTHOR INFORMATION

Corresponding Author

*Phone: +34 958 23 00 00 (ext. 190123). Fax: +34 958 55 26 20. E-mail: chiaracappelli@ugr.es.

Notes

The authors declare no competing financial interest.

■ ACKNOWLEDGMENTS

Financial support was obtained from Projects CGL2008-01652 and CGL2011-22567 (Plan Nacional I+D and EU). C.C. benefitted from a FPU grant (MEC), and A.E.S.V.D. is grateful for the support by the Consolider-Ingenio 2010 project "Factoría Española de Crystalización". Luis David Patiño López is acknowledged for his assistance during the experimental work. The comments and suggestions of Dr. Felix Brandt and two anonymous reviewers have largely improved the quality of the manuscript and are gratefully acknowledged.

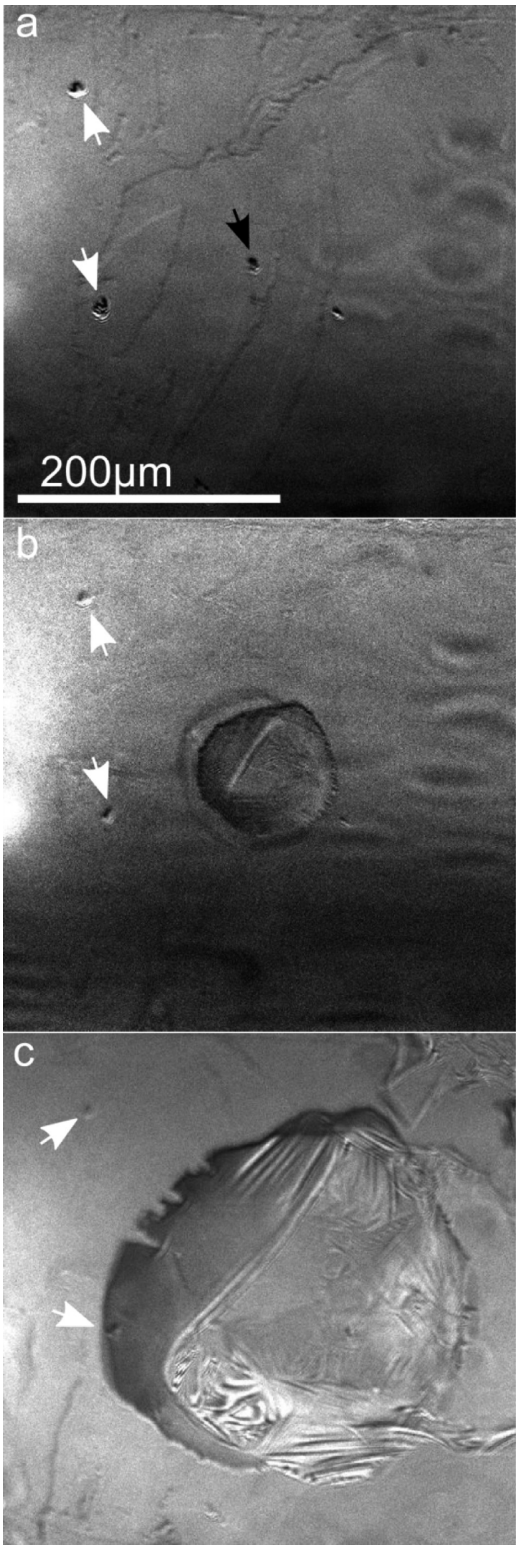

Figure 5. LCM-DIM images of biotite (001) cleavage surface: pristine surface with a visible defect indicated by the black arrow (a); same surfaces after ~7.5 h (b) and after 23 h (c) of reaction at pH 1 and 25 °C. Dissolution proceeded from the edge surface of the defect (hole). White arrows indicate holes that did not react, most likely because they were below the upper layer that interacted with solution.

Table 2. Horizontal-Retreat Rates (R_r) Calculated from the Horizontal Surface Retreat of the Lower Steps at the Respective Temperature

T (°C)	R_r (μm s^{-1})
11.5	7.5×10^{-4}
25	3.5×10^{-3}
40	1.9×10^{-2}
50	2.6×10^{-2}
70	6.2×10^{-2}

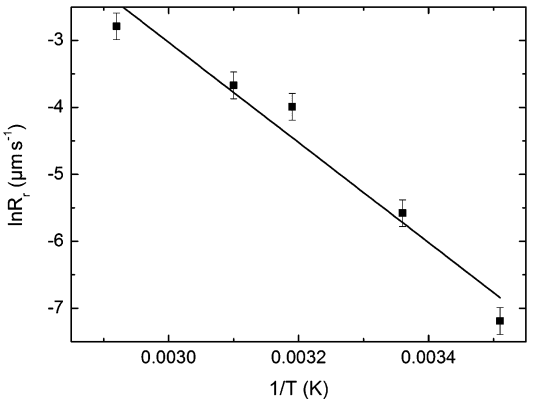

Figure 6. Arrhenius plot calculated from measurement of horizontal retreat rates at pH 1 and 11.5 to 70 °C (R^2 = 0.96).

REFERENCES

(1) Brantley, S. L. In *Kinetics of Water-Rock Interaction*; Brantley, S. L., Kubicki, J. D., White, A. F., Eds.; Springer: New York, 2008; pp 151–210.

(2) Brantley, S. L.; Conrad, C. F. In *Kinetics of Water-Rock Interaction*; Brantley, S. L., Kubicki, J. D., White, A. F., Eds.; Springer: New York, 2008; pp 1–38.

(3) Ganor, J.; Mogollón, J. L.; Lasaga, A. C. *Geochim. Cosmochim. Acta* **1995**, *59*, 1037–1052.

(4) Acker, J. G.; Bricker, O. P. *Geochim. Cosmochim. Acta* **1992**, *56*, 3073–3092.

(5) Kalinowski, B. E.; Schweda, P. *Geochim. Cosmochim. Acta* **1996**, *60*, 367–385.

(6) Turpault, M. P.; Trotignon, L. *Geochim. Cosmochim. Acta* **1994**, *58*, 2761–2775.

(7) Rufe, E.; Hochella, M. F., Jr. *Science* **1999**, *285*, 874–876.

(8) Bosbach, D.; Charlet, L.; Bickmore, B.; Hochella, M. F., Jr. *Am. Mineral.* **2000**, *85*, 1209–1216.

(9) Bickmore, B. R.; Bosbach, D.; Hochella, M. F., Jr.; Charlet, L.; Rufe, E. *Am. Mineral.* **2001**, *86*, 411–423.

(10) Aldushin, K.; Jordan, G.; Schmahl, W. W. *Geochim. Cosmochim. Acta* **2006**, *70*, 4380–4391.

(11) McMaster, T. J.; Smits, M. M.; Haward, S. J.; Leake, J. R.; Banwart, S.; Ragnarsdottir, K. V. *Mineral. Mag.* **2008**, *72*, 115–120.

(12) Haward, S. J.; Smits, M. M.; Ragnarsdóttir, K. V.; Leake, J. R.; Banwart, S. A.; McMaster, T. J. *Geochim. Cosmochim. Acta* **2011**, *75*, 6870–6881.

(13) Pachana, K.; Zuddas, P.; Censi, P. *Appl. Geochem.* **2012**, *27*, 1738–1744.

(14) Sazaki, G.; Matsui, T.; Tsukamoto, K.; Usami, N.; Ujihara, T.; Fujiwara, K.; Nakajima, K. *J. Cryst. Growth* **2004**, *262*, 536–542.

(15) Van Driessche, A. E. S.; Otálora, F.; Sazaki, G.; Sleutel, M.; Tsukamoto, K.; Gavira, J. A. *Cryst. Growth Des.* **2008**, *8*, 4316–4323.

(16) Van Driessche, A. E. S.; García-Ruiz, J. M.; Delgado-Lpez, J. M.; Sazaki, G. *Cryst. Growth Des.* **2010**, *10*, 3909–3916.

(17) Van Driessche, A. E. S.; Gavira, J. A.; Patiño Lopez, L. D.; Otalora, F. *J. Cryst. Growth* **2009**, *311*, 3479–3484.

(18) Brandt, F.; Bosbach, D.; Krawczyk-Bärsch, E.; Arnold, T.; Bernhard, G. *Geochim. Cosmochim. Acta* **2003**, *67*, 1451−1461.
(19) Kaviratna, H.; Pinnavaia, T. J. *Clays Clay Miner.* **1994**, *42*, 717−723.
(20) Lasaga, A. C. *Kinetic Theory in the Earth Sciences*; Princeton University Press: New Jersey, 1998.